Generic membrane-spanning features endow IRE1α with responsiveness to membrane aberrancy

Nozomu Kono†*, Niko Amin-Wetzel, and David Ron*
Cambridge Institute for Medical Research, University of Cambridge, Cambridge CB2 0XY, United Kingdom

ABSTRACT **Altered cellular lipid composition activates the endoplasmic reticulum unfolded protein response (UPR), and UPR signaling effects important changes in lipid metabolism. Secondary effects on protein folding homeostasis likely contribute to UPR activation, but deletion of the unfolded protein stress-sensing luminal domain of the UPR transducers PERK and IRE1α does not abolish their responsiveness to lipid perturbation. This finding suggests that PERK and IRE1α also directly recognize the membrane aberrancy wrought by lipid perturbation. However, beyond the need for a transmembrane domain (TMD), little is known about the features involved. Regulation of the UPR transducers entails changes in their oligomeric state and is easily corrupted by overexpression. We used CRISPR/Cas9-mediated gene editing of the *Ern1* locus to study the role of the TMD in the ability of the endogenous IRE1α protein to recognize membrane aberrancy in mammalian cells. Conducted in the background of a point mutation that isolated the response to membrane aberrancy induced by palmitate from unfolded protein stress, our analysis shows that generic membrane-spanning features of the TMD are sufficient for IRE1α's responsiveness to membrane aberrancy. Our data suggest that IRE1α's conserved TMD may have been selected for features imparting a relatively muted response to acyl-chain saturation.**

Monitoring Editor
Reid Gilmore
University of Massachusetts

Received: Mar 14, 2017
Revised: Jun 7, 2017
Accepted: Jun 9, 2017

This article was published online ahead of print in MBoC in Press (http://www.molbiolcell.org/cgi/doi/10.1091/mbc.E17-03-0144) on June 14, 2017.

†Present address: Graduate School of Pharmaceutical Sciences, University of Tokyo, Tokyo 113-0033, Japan.

*Address correspondence to: Nozomu Kono (nozomu@mol.f.u-tokyo.ac.jp), David Ron (dr360@medschl.cam.ac.uk).

N.K. co-led the study, designed and performed the bulk of the experiments, and cowrote the manuscript. N.A.-W. contributed to experimental design and interpretation, coedited the manuscript, and pioneered the methods used to edit the *Ern1* locus in CHO cells and select informative derivative subclones based on their phenotype. D.R. co-led the study and participated in experimental design, contributed to the interpretation of data, and cowrote the manuscript.

Abbreviations used: 2DG, 2-deoxy-D-glucose; 4-PBA, 4-phenyl butyrate; AH, amphipathic helix; BSA, bovine serum albumin; CHOP, C/EBP homologous protein; CNX, calnexin; CRISPR, clustered regularly interspaced short palindromic repeats; ER, endoplasmic reticulum; FACS, fluorescence-activated cell sorting; GFP, green fluorescent protein; HDR, homology-directed repair; HEPES, 4-(2-hydroxyethyl)-1-piperazineethanesulfonic acid; InDels, insertions or deletions; IRE1, inositol requiring 1; LD, luminal domain; MFI, median fluorescence intensity; *Mr*, relative molecular mass; PA, palmitate; PBS, phosphate-buffered saline; PERK, PKR-like ER kinase; sgRNA, single-guide RNA; SP, signal peptide; TM, transmembrane; Tm, tunicamycin; TMD, TM domain; UPR, unfolded protein response; WT, wild type; XBP1, X-box binding protein-1.

INTRODUCTION

The endoplasmic reticulum (ER) unfolded protein response (UPR) modulates protein synthesis and gene expression to match the protein-folding capacity of the early secretory pathway to the compartment-specific burden of unfolded proteins. However, the UPR is also powerfully activated by changes in cellular lipid composition (Cox *et al*., 1997; Li *et al*., 2004; Pineau *et al*., 2009; Ariyama *et al*., 2010), a feature conserved in eukaryotes (reviewed in Volmer and Ron, 2015). The functional significance of UPR activation by lipid perturbation is amply supported by physiological and genetic observations: inositol requiring 1 (IRE1), the sole transducer of UPR signaling in yeast, is powerfully activated by depletion of the yeast membrane precursor inositol (Cox *et al*., 1997) and by diverse lipid perturbations caused by gene deletion (Jonikas *et al*., 2009). As suggested by its name, IRE1 signaling is essential for replenishing inositol stores. This is reflected by the auxotrophic features of deletion of either the upstream sensor-transducer IRE1 or its downstream effector, the transcription factor Hac1p/inositol requiring 2 (Ire2p; Nikawa and Yamashita, 1992; Cox *et al*., 1997). Enzymes involved in lipid synthesis and metabolism are regulated by the UPR in both yeast (Travers *et al*., 2000) and animals (Sriburi *et al*., 2004; Adamson *et al*., 2016). Interest in lipid-driven UPR signaling is fueled both by curiosity regarding the fundamentals of the aforementioned

cross-talk and evidence that activation of the pathway might play a role in common diseases of metabolism, such as atherosclerosis (Feng *et al.*, 2003), diabetes mellitus (Cunha *et al.*, 2008), and fatty liver disease (Fu *et al.*, 2011; reviewed in Han and Kaufman, 2016).

Altering membrane lipid composition has pleiotropic effects on cells (Thibault *et al.*, 2012), including corruption of both calcium signaling (Li *et al.*, 2004; Fu *et al.*, 2011) and thiol redox (Cunha *et al.*, 2008), either of which stands to influence protein-folding homeostasis in the ER indirectly. However, a pioneering experiment in yeast showed that Ire1p retains the ability to respond to inositol depletion despite a deletion in its luminal stress-sensing domain that severely compromises the response to protein misfolding (Promlek *et al.*, 2011). Similarly, mutant derivatives of the animal-cell UPR transducers PKR-like ER kinase (PERK) and IRE1α that lack their stress-sensing luminal domain and hence are unresponsive to unfolded protein stress nonetheless retain responsiveness to perturbation of cell lipid composition (Volmer *et al.*, 2013). Responsiveness to lipids was completely dependent on membrane association of these mutant stress transducers, as cytosolic derivatives of the effector domain (lacking a membrane anchor) were inactive (Volmer *et al.*, 2013). That a response of the UPR transducers to lipids might exist independently of unfolded protein signaling is also supported by the observation that chemical chaperones such as 4-phenylbutyric acid and tauroursodeoxycholate selectively interfere with IRE1α activation by unfolded proteins but not by saturated fatty acids (Robblee *et al.*, 2016). Together these observations support the idea that some types of membrane aberrancy are recognized by the UPR transducers, as suggested originally (Promlek *et al.*, 2011).

Transmembrane (TM) segments have long been known to underlie cellular responsiveness to changes in membrane lipid composition, as exemplified by the multipass sterol-sensing domain of 3-hydroxy-3-methylglutaryl coenzyme A (HMG-CoA) reductase, the rate-limiting enzyme in sterol biosynthesis (Gil *et al.*, 1985). Even a single TM domain (TMD) can register the effect of changes in membrane thickness (Cybulski *et al.*, 2010; Sharpe *et al.*, 2010), cholesterol, ganglioside, or sphingolipid content (Coskun *et al.*, 2011; Contreras *et al.*, 2012), or acyl-chain saturation/lipid packing (Covino *et al.*, 2016). The sequence of the TMD may be important, as exemplified by p24 (an element of the COP I machinery), for which a TM motif links sphingolipid binding to changes in p24 oligomeric state (Contreras *et al.*, 2012). In a different example, features of the TMD of the ER-anchored yeast transcription factor Mga2p modulate homotypic rotational interactions between the TMDs of adjacent molecules in response to changes in lipid packing (Covino *et al.*, 2016). These findings and a large body of reductionist biophysical studies (reviewed in Lee, 2011) point to the importance of TMD sequence-dependent recognition of changes in membrane lipid composition.

The essential role of a TMD in IRE1α's ability to recognize membrane aberrancy (Volmer *et al.*, 2013) fits well with evidence for sensitivity of UPR induction to acyl chain length, level of unsaturation, position of the double bonds, and their isomerization (Deguil *et al.*, 2011; Surma *et al.*, 2013). However, important methodological limitations previously precluded a critical analysis of features of IRE1α's TMD that might recognize membrane aberrancy. First, UPR activation was measured by X-box binding protein-1 (XBP1) mRNA splicing, an assay of low throughput that limited a detailed analysis of dose–response relationships. Second, mutant IRE1α proteins were analyzed by ectopically expressing them from transgenes in *Ern1*-knockout cells. Although this successfully negated contribution from the wild-type allele, it was impossible to reliably achieve physiological (low) levels of IRE1α expression, nor was it possible to account for overexpression and the corrupting effect it has on IRE1α activity (a highly concentration-dependent process; Korennykh *et al.*, 2011). Drawing on recent developments in clustered regularly interspaced short palindromic repeats (CRISPR)/Cas9 gene editing, we addressed these limitations and report on the response to lipid aberrancy of a range of IRE1α TMD mutants expressed from the endogenous *Ern1* locus of isogenic CHO-K1 cells endowed with sensitive fluorescence-based UPR reporters with a broad dynamic range.

RESULTS

Experimental platform to study membrane aberrancy–mediated IRE1α signaling

To explore the role of IRE1α in responding to membrane aberrancy, we exploited a CHO-K1–derived cell line (S21) containing both a C/EBP homologous protein (CHOP)::green fluorescent protein (GFP) transcriptional reporter of the UPR PERK-dependent branch (Novoa *et al.*, 2001) and an mRNA-based XBP1s::Turquoise reporter responsive to IRE1α's sequence-specific RNase activity (based on Iwawaki *et al.*, 2004). Flow cytometry analysis of cells treated with either tunicamycin or 2-deoxy-D-glucose (2DG; to perturb protein-folding homeostasis in the ER) or palmitate (a saturated fatty acid, to promote membrane aberrancy) showed that in these cells, all three agents activated both strands of the UPR in a concentration-dependent manner. In most experiments, activation of the XBP1s::Turquoise reporter did not saturate, even at the highest concentrations of palmitate that were compatible with cell viability (Figure 1). Nonetheless, the ascending limb of the concentration–response curve was deemed broad enough to enable study of the IRE1α branch of the UPR.

To explore the role of IRE1α's TMD in responding to membrane aberrancy, we first used CRISPR/Cas9-mediated gene editing to introduce frameshifting mutations into the TMD-encoding region of the two chromosomal copies of *Ern1*. As expected, the resulting inactivation of IRE1α in the ΔTM12 clone led to selective loss of the XBP1s::Turquoise signal in stressed cells and only a modest attenuation of the mostly PERK-dependent CHOP::GFP signal (Figure 2A and Supplemental Figure S2, A–C). Retargeting the mutant *Ern1* locus of ΔTM12 clone with CRISPR/Cas9 and a repair template encoding the wild-type TMD restored stress-dependent activation of XBP1s::Turquoise on a discernible fraction of the cells (Figure 2B, left). "Rescued" cells were segregated by fluorescence-activated cell sorting (FACS) of the XBP1s::Turquoise$^+$ population (their recovery as viable clonogenic cells was greatly facilitated by exploiting the reversible action of 2DG) and subsequently analyzed either as an expanded polyclonal pool or as individual rescued clones (Figure 2B, right).

Functional consequences of sequence modifications of the endogenous IRE1α's TMD

The aforementioned experimental system was used to explore features of IRE1α's highly conserved TMD (Supplemental Figure S2D) that might be relevant to recognizing membrane aberrancy. Offering a repair template that encoded either a wild-type or a sequence-scrambled (similar to that used in Volmer *et al.*, 2013) IRE1α TMD to the retargeted ΔTM12 cells generated isogenic cells that differed only in the sequence of the portion of the *Ern1* gene encoding IRE1α TMD (Figure 3A). Levels of IRE1α expression varied in retargeted, rescued, ΔTM12 clones (Figure 3B). This variation likely reflected the combined effects of gene dosage and properties of the rescued allele. Through genotypic analysis, we confined the downstream studies to clones that had a single detectable allele (encoding either a wild-type or a scrambled TMD). However, with the tools available to us, we were unable to distinguish between cells having two rescued *Ern1* alleles and cells having one rescued allele in-*trans* to a large deletion that was not detected in the

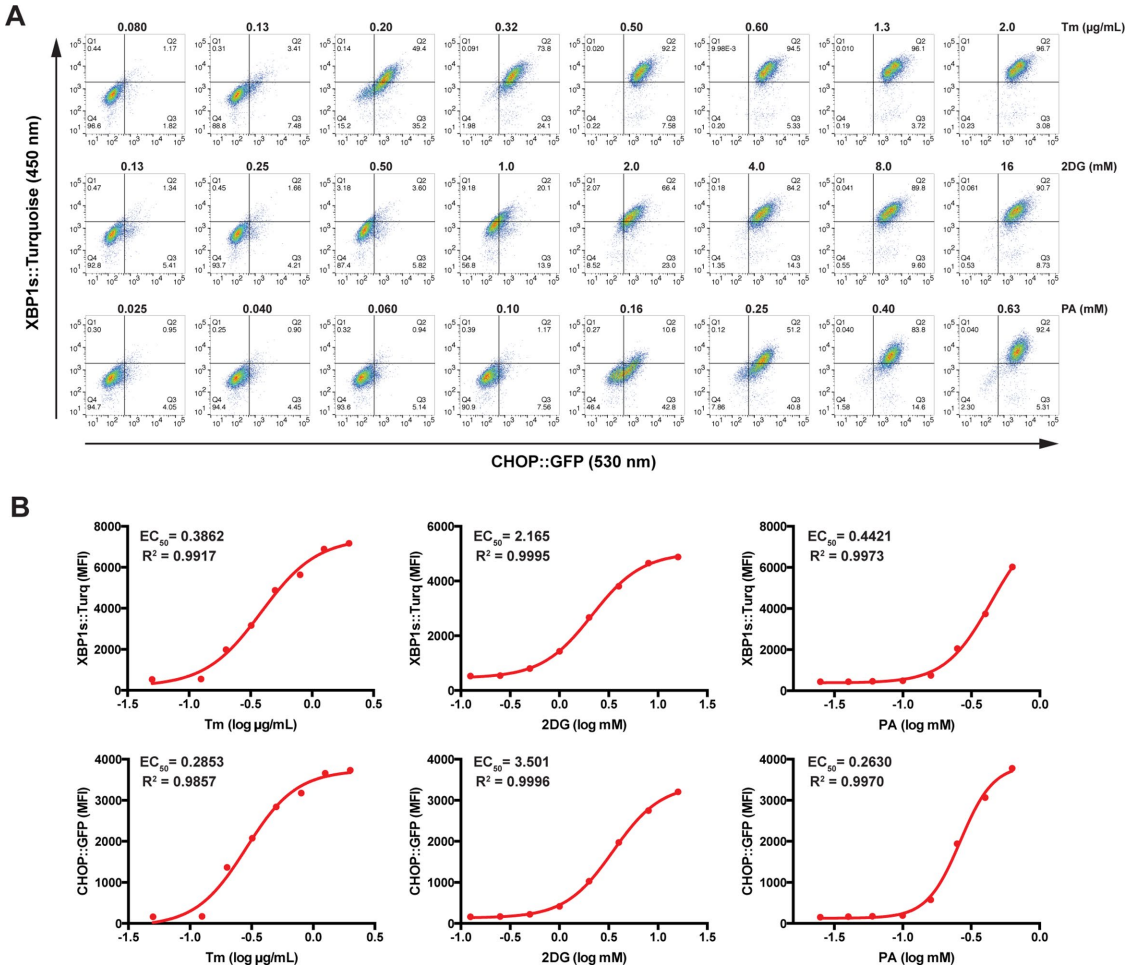

FIGURE 1: Dual UPR pathway reporter cell line for tracking UPR activity induced by unfolded protein stress and lipid aberrancy with a broad dynamic range. (A) Flow cytometry analysis of XBP1s::Turquoise (XBP1s::Turq) and CHOP::GFP expression in a dual UPR reporter cell line (S21 cells) treated with various concentrations of tunicamycin (Tm), 2DG, or palmitate (PA) for 24 h. (B) Dose–response curve of UPR reporter expression in S21 cells treated with Tm, 2DG, or PA at concentrations as in A for 24 h. Median fluorescence intensities (MFI, in arbitrary units) for at least 9×10^3 cells were measured by flow cytometry. Curves were fitted to a four-parameter logistic model. Half-maximal effective concentration (EC_{50}) and coefficient of determination (R^2).

fragment-based genotypic analysis (see *Materials and Methods*). Thus clone TM-WT-16 is likely homozygous for wild-type *Ern1 allele* (having wild-type levels of IRE1α protein and a wild-type response to stress), whereas clone TM-WT-22 is likely heterozygous for wild-type and null *Ern1* alleles. Zygosity of the scrambled TMD clones (SC-4 and SC-8) cannot be guessed at; however, assuming that the subtle sequence differences between the wild-type and scrambled repair template had no effect on the relative recovery of cells with one rescued *Ern1* allele and with two rescued *Ern1* alleles, the lower levels of IRE1α protein observed in the polyclonal pool of cells rescued with the scrambled allele suggests that the latter encoded a protein that accumulated to lower levels in cells (Figure 3B, left).

Despite the lower levels of expression of the scrambled IRE1α, both wild-type and scrambled TMD-rescuing alleles gave rise to similar profiles of activity in cells treated with tunicamycin, 2DG, and, remarkably, palmitate. This was evident both by comparing polyclonal populations of ΔTM12 cells rescued with the wild-type and scrambled TMD–encoding repair templates (Figure 3C and Supplemental Figure S3A) and by studying the features of individual clones (Figure 3D and Supplemental Figure S3B). These findings speak against a stringent requirement for the arrangement of the side chains of the TMD in IRE1α function.

Covino *et al.* (2016) described features of the TMD of the yeast ER-tethered transcription factor Mga2p that endow it with sensitivity to changes in lipid packing wrought by altering acyl-chain saturation. They drew attention to the role of bulky aromatic residues, such as tryptophan and phenylalanine, and to the presence of proline residues in favoring alternative conformations of the Mga2p TMD dimer in more loosely packed and more ordered membranes constituted of unsaturated and saturated lipids, respectively. These features of Mga2p contribute to lipid homeostasis in yeast by coupling expression of *OLE1*, the gene encoding a fatty acid desaturase, to changes in membrane lipid saturation (Covino *et al.*, 2016). Furthermore, Russ and Engelman (2000) pointed out the importance of an interrupted diglycine motif in homodimerizing TMD.

IRE1α has a conserved tryptophan, phenylalanine, tyrosine, and proline in its TMD (Supplemental Figure S2D), as well as an interrupted glycine and alanine motif whose presence was unaffected by scrambling (Figure 3A). To determine whether these residues contributed to sensing of membrane aberrancy by IRE1α, we reconstituted

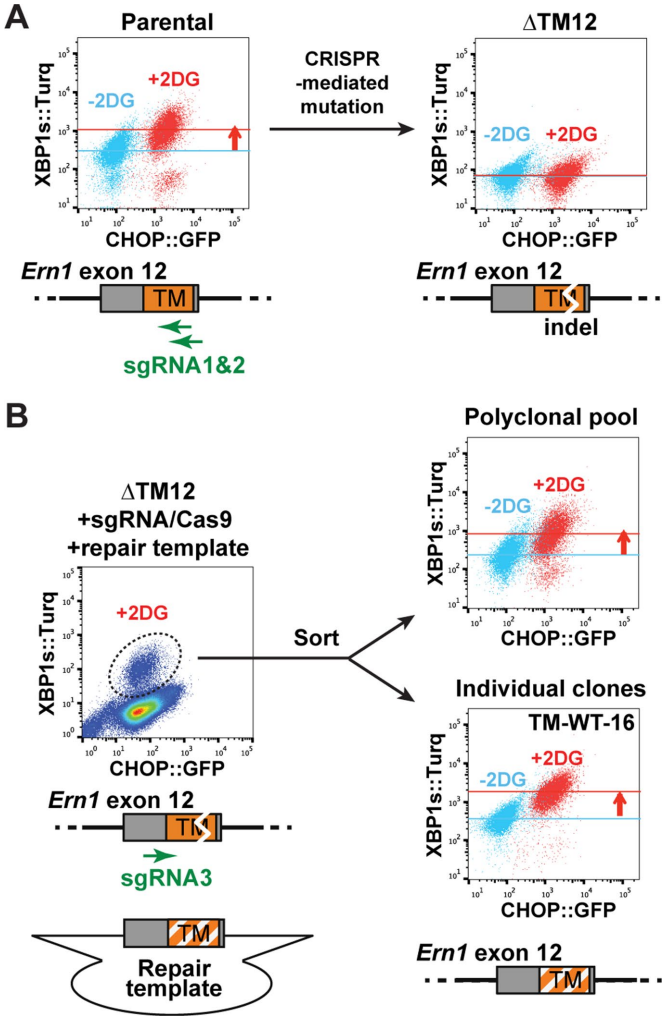

FIGURE 2: Deletion and reconstitution of IRE1α's TMD by CRISPR/Cas9 gene editing. (A) Flow cytometry analysis of cells untreated (blue) and treated with 4 mM 2DG for 24 h (red). Left, parental S21 (wild-type) cells; right, mutant ΔTM12 cells with CRISPR/Cas9-mediated gene-disrupting InDels in the TMD. A schema for the IRE1α-encoding *Ern1* gene and the position of the guide RNAs that target Cas9 are shown below the plots. Gray boxes indicate exon 12, and orange boxes indicate the coding sequence of the IRE1α TMD. (B) Flow cytometry analysis of ΔTM12 cells retargeted with a guide RNA directed to the mutant exon 12 and a repair template that restores the wild-type (WT) TMD. ΔTM12 cells successfully reconstituted with WT IRE1 (encircled by broken line) were distinguished from the rest of the population by 2DG treatment and collected using FACS. Top right, resultant polyclonal populations, both untreated and treated with 2DG. Bottom right, representative single clone of the rescued cells.

the endogenous locus of the nullizygous ΔTM12 clone with mutant versions of *Ern1* encoding IRE1α proteins lacking these key features (Figure 4, A and B). Although the mutants varied in their ability to activate the XBP1s::Turquoise reporter, none exhibited a selective defect in response to lipid aberrancy (Figure 4, C and D, and Supplemental Figure S4). Even a mutant in which all of the predicted membrane-spanning residues had been replaced by leucines, IRE1α$^{TM>L}$, retained a hierarchy of response to palmitate, 2DG, and tunicamycin that resembled the wild type. For all mutants tested, endurance of the response to membrane aberrancy was noted at levels of expressions that either matched or were lower than those of the wild-type IRE1α. This was especially conspicuous in the IRE1α$^{TM>L}$, which reproducibly gave the weakest signal in the immunoprecipitation-immunoblot (Figure 4B).

The region immediately N-terminal to the IRE1α TMD is predicted to form an amphipathic extension of the membrane-spanning helix, a feature conserved in the yeast Ire1p (Figure 5A and Supplemental Figure S5, A and B). It has been proposed that hydrophobic side chains of residues from one face of this predicted amphipathic helix are inserted into the lipid bilayer, constraining the TMD in a manner that favors dimerization in an ordered bilayer (Halbleib *et al.*, 2017). To examine the role of these residues in the responsiveness of IRE1α to lipid aberrancy, we reconstituted the endogenous locus with mutant versions of *Ern1* encoding IRE1α proteins in which the amphipathic features of this region were disrupted (this was archived by exploiting *Ern1*$^{\Delta LD15}$, a signaling-defective allele of IRE1α described later). Of note, both the IRE1α^{V437R} and IRE1α^{L441R} mutant proteins retained wild-type levels of inducibility by palmitate, 2DG, and tunicamycin (Figure 5, B and C, and Supplemental Figure S5C). Although we have not examined this aspect experimentally, the elevated basal activity of the XBP1s::Turquoise reporter reproducibly noted in the IRE1α^{L441R} mutant cells might be explained by the loss of a repressive contact with the Sec61 complex (Sundaram *et al.*, 2017).

The IRE1α^{Y161A} mutation selectively enfeebles the response to unfolded protein stress, exposing IRE1α's ability to sense membrane aberrancy

The experimental observations presented so far speak against an important role for the side chains of specific TMD residues (and TMD-proximal residues of the predicted N-terminal amphipathic helix) in endowing IRE1α with the ability to recognize membrane aberrancy imposed by culturing cells in a range of concentrations of palmitate. However, as noted in the *Introduction*, manipulation of membrane lipid composition has pleiotropic effects that might include induction of unfolded protein stress in the ER lumen. The observed indifference of IRE1α to mutations in its TMD might therefore reflect dominance of the unfolded protein stress over membrane aberrancy in the forces that act on IRE1α in palmitate-exposed CHO-K1 cells. Our efforts to address this possibility by selectively buffering the consequences of protein misfolding with a chemical chaperone, 4-phenyl butyrate (4-PBA), were frustrated by the fact that at the concentrations required to attenuate UPR induction by tunicamycin, 4-PBA nonspecifically suppressed unrelated stress signaling. Therefore we sought to create an IRE1α allele that was selectively compromised in its ability to respond to unfolded protein stress over its response to membrane aberrancy.

Using CRISPR/Cas9, we created a CHO-K1 cell line with an in-frame deletion allele of *Ern1* encompassing the entire coding sequence of the stress-sensing luminal domain of IRE1α (in-*trans* to a larger deletion that disrupts the coding sequence, *Ern1*$^{\Delta LD15/null}$; Figure 6, A and B, and Supplemental Figure S6, A–C). Overexpression of a transgene encoding a similar protein imparted selective responsiveness to palmitate loading upon *Ern1*-deleted mouse cells (Volmer *et al.*, 2013). However, although detectable, the IRE1α$^{\Delta LD}$ protein encoded by the mutant *Ern1*$^{\Delta LD15}$ locus failed to activate the XBP1s::Turquoise reporter in palmitate-treated cells (Supplemental Figure S6D; the minimal increase in XBP1s::Turquoise of palmitate-treated ΔLD15 cells likely reflects a process unrelated to IRE1α-mediated splicing, as it was also observed in the ΔTM12 cells lacking all IRE1α function [Supplemental Figure S2C]). This observation is consistent with a role for luminal domain–mediated dimerization in the responsiveness of IRE1α to membrane aberrancy when expressed at physiological levels, a requirement that is bypassed by

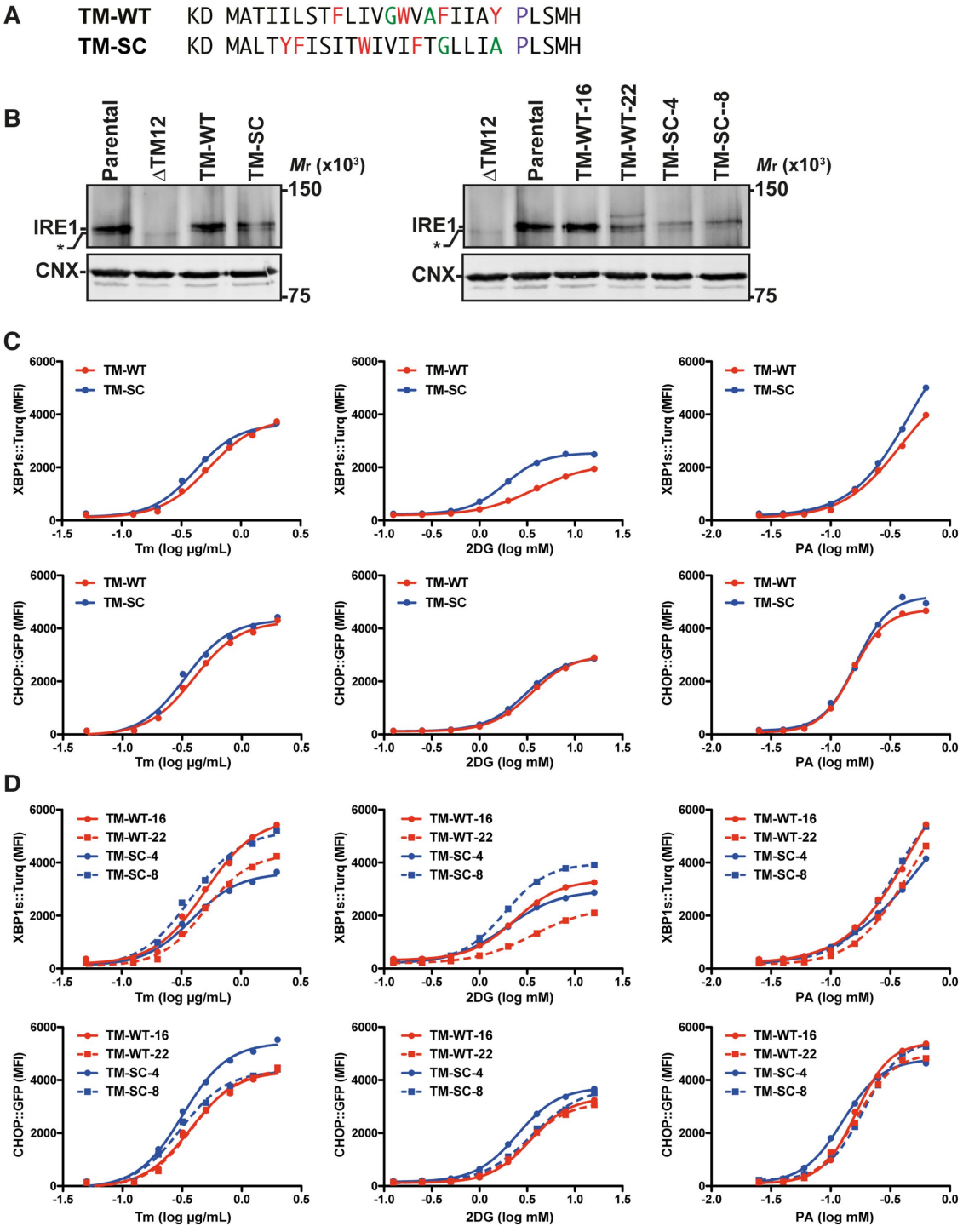

FIGURE 3: TMD-scrambled IRE1α responds to palmitate. (A) Sequence comparison of the wild-type (TM-WT) and scrambled (TM-SC) TMDs of IRE1α. Aromatic residues (red), GXXXG-like motif (green), and proline (purple). (B) Immunoblot of IRE1α protein immunoprecipitated from detergent lysates of parental (S21), ΔTM12, and polyclonal pools (left) or individual clones (right) of TMD-reconstituted cells. Cells were first permeabilized with 0.09% digitonin to lower the background from cytosolic proteins and soluble mutant IRE1α lacking a TMD, solubilized in 1% Triton X-100, and analyzed by immunoprecipitation/Western blot with anti-IRE1α antibody or Western blot with anti-calnexin (CNX) antibody (used as a loading control; bottom). Asterisks indicate a nonspecific band superimposed on the residual signal from mutant IRE1α lacking a TMD (from skipping of the mutant exon 12). *Mr*, relative molecular mass. Blots are representative of at least two independent experiments. (C, D) Dose– response curve of UPR reporter activity in polyclonal pools (C) or individual clones (D) of IRE1α TMD-reconstituted cells treated with Tm, 2DG, or PA at concentrations as in Figure 1A for 24 h. MFI for at least 9×10^3 cells was measured by flow cytometry. Curves were fitted to a four-parameter logistic model. Data are representative of three independent experiments (two other experiments are shown in Supplemental Figure S3).

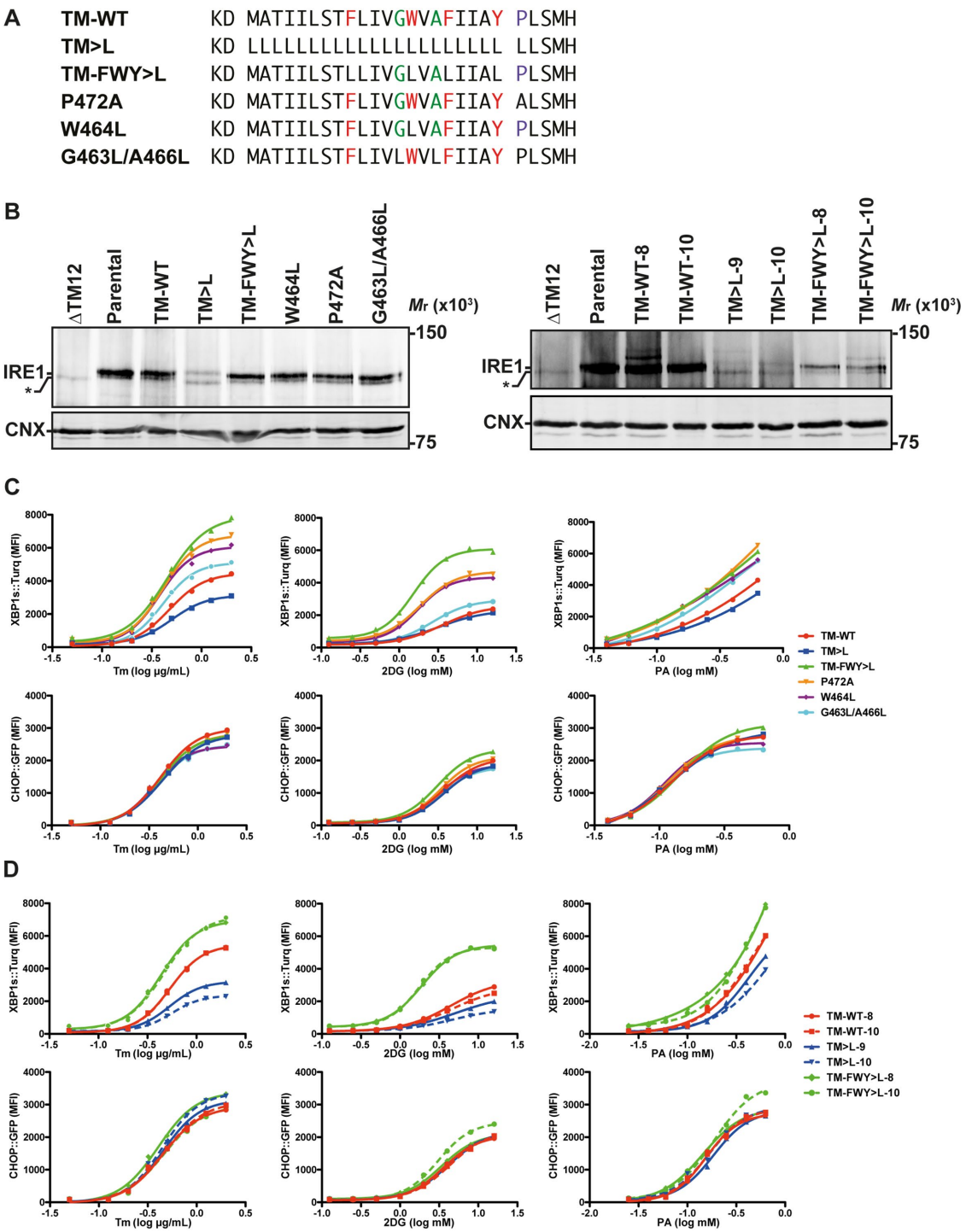

FIGURE 4: Generic features of the TMD are sufficient for sensing membrane aberrancy. (A) Sequences of the IRE1α wild-type (WT) and various TMD mutants studied. Aromatic residues (red), GXXXG-like motif (green), and proline (purple). TM>L indicates an IRE1 mutant whose TMD consists of only leucine residues. In FWY>L, the aromatic residues were replaced with leucine residues. (B) Immunoblot of IRE1α and CNX (a loading control) from the TMD-reconstituted cells (as in Figure 3B). Cells were permeabilized with 0.09% digitonin, solubilized, and analyzed by immunoprecipitation/Western blot with anti-IRE1α antibody or Western blot with anti-CNX antibody. Asterisks indicate nonspecific bands. *Mr*, relative molecular mass. Blots are representative of at least two independent experiments. (C, D) Dose–response curve of UPR reporter expression in polyclonal pools (C) or individual clones (D) of IRE1α TMD-reconstituted cells treated with Tm, 2DG, or PA at concentrations as in Figure 1A for 24 h. MFI for at least 9×10^3 cells was measured by flow cytometry. Curves were fitted to a four-parameter logistic model. Data are representative of three independent experiments (two other experiments are shown in Supplemental Figure S4).

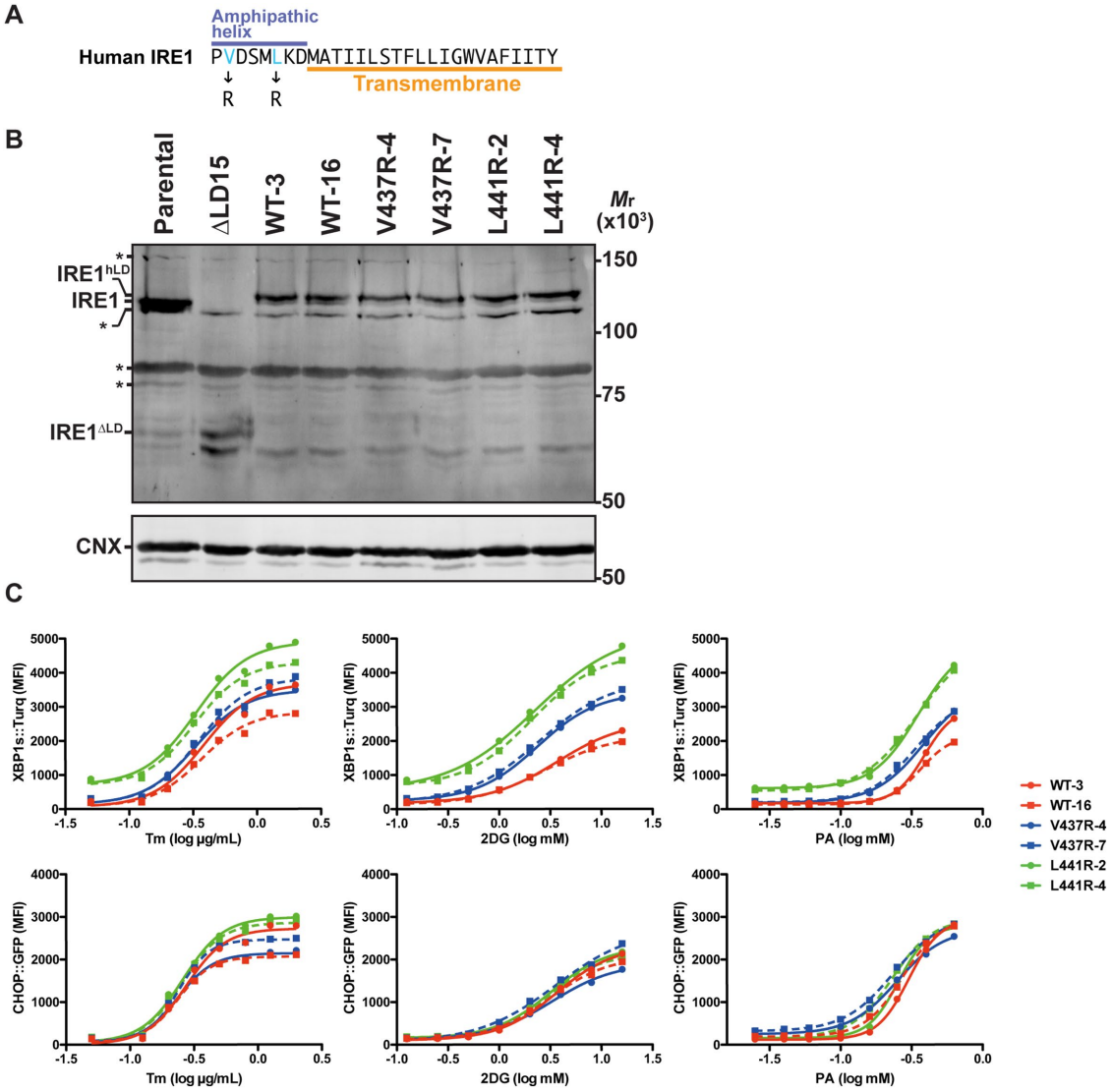

FIGURE 5: Amphipathic helix mutants of IRE1α respond to palmitate stress. (A) Sequence of the predicted amphipathic helical (AH) extension of IRE1α TMD. Hydrophobic residues mutated in the experiments below are colored cyan. (B) Immunoblot of IRE1α and CNX (a loading control) from the TMD-reconstituted cells (as in Figure 3B). ΔLD15 cells express an IRE1α protein with a large deletion encompassing the luminal domain (see Supplemental Figure 6A for further details); they serve as a platform for reconstituting with the other TMD mutants shown here. Blots are representative of at least two independent experiments. (C) Dose–response curve of UPR reporter expression in individual clones of IRE1α AH mutant cells treated with Tm, 2DG, or PA at concentrations as in Figure 1A for 24 h. MFI for at least 9×10^3 cells was measured by flow cytometry. Curves were fitted to a four-parameter logistic model. Data are representative of at least two independent experiments (another experiment is shown in Supplemental Figure S5).

overexpression. Retargeting the *Ern1*$^{\Delta LD15}$ locus with CRISPR/Cas9 while offering a human cDNA ("minigene")-based repair template (encompassing exons 2–12 and encoding the wild-type luminal domain of human IRE1α) restored IRE1α activity in tunicamycin-, 2DG-, and palmitate-treated cells (Figure 6C and Supplemental Figure S6C). Of importance, when a repair template encoding an IRE1α^{Y161A} mutation (corresponding to yeast Ire1p^{F285A}; Credle *et al.*, 2005; Zhou *et al.*, 2006) was used in place of the wild type, activation of XBP1s::Turquoise by tunicamycin or 2DG was lost, but a measure of response to palmitate loading reproducibly remained (Figure 6, C and D, and Supplemental Figure S6, E–G). The residual responsiveness of IRE1α^{Y161A} to palmitate was clearly a feature of the mutant luminal domain, as it was absent from the parental ΔLD15 cells (Supplemental Figure S6E). These findings indicate that the Y161A mutation in IRE1α drives a wedge between the responsiveness to unfolded proteins and membrane aberrancy at levels of expression that are lower than the wild type. The mechanism by which the Y161A mutation interferes with IRE1α's responsiveness to unfolded protein stress remains to be determined; nonetheless, this point mutation provides a platform for selectively testing the effect of secondary mutations on IRE1α's ability to recognize membrane aberrancy.

Membrane aberrancy is robustly sensed by TMD-mutant IRE1α

Building on this finding, we retargeted the *Ern1*$^{\Delta LD15}$ locus with CRISPR/Cas9 while offering a human cDNA ("minigene")-based

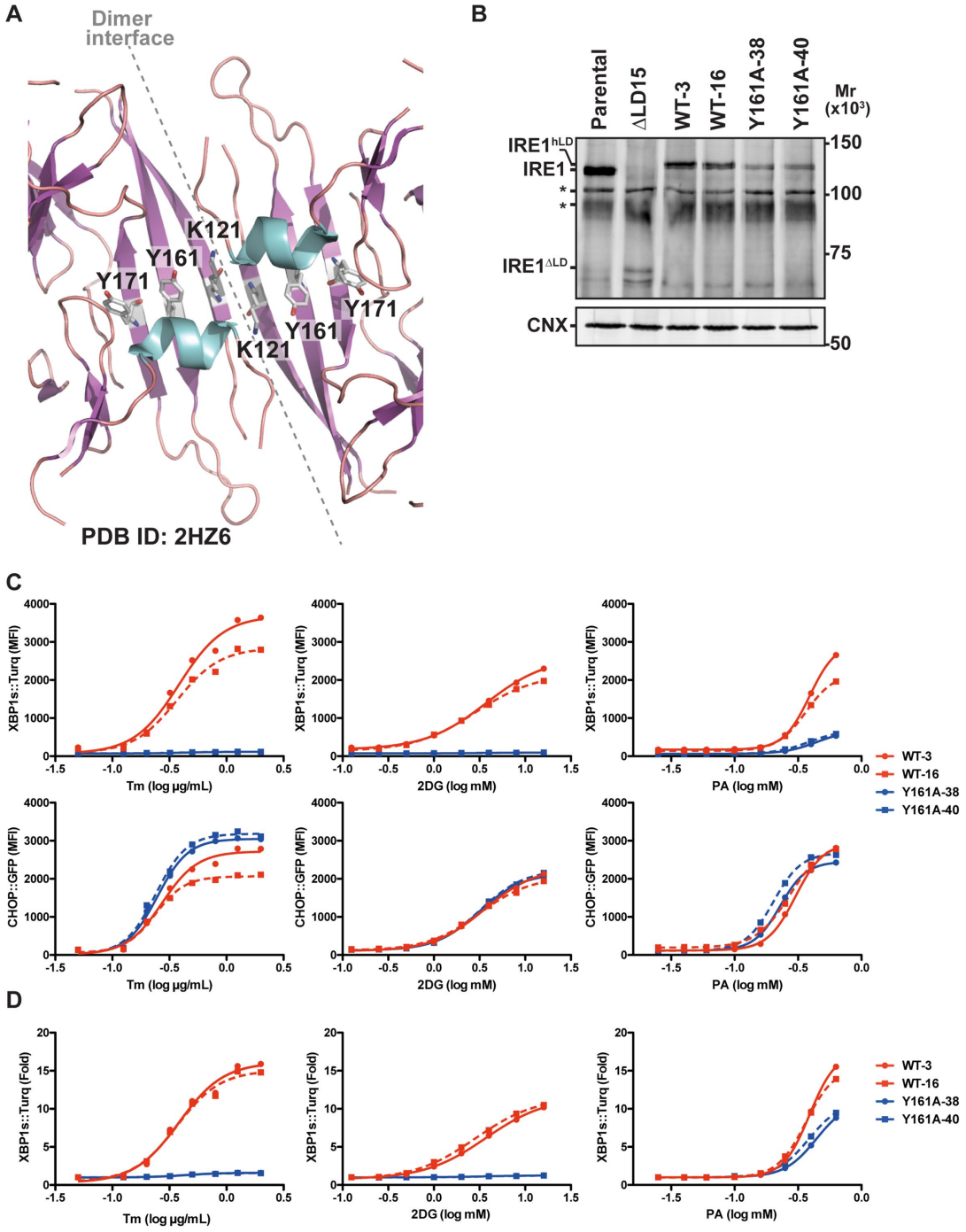

FIGURE 6: IRE1α^{Y161A} responds to palmitate but not to unfolded protein stress. (A) Cartoon representation of crystal structure of human IRE1α luminal domain (LD; Protein Data Bank ID: 2HZ6). α-Helices, β-strands, and loops are colored cyan, magenta, and wheat, respectively. Counterparts to residues involved in the response of yeast Ire1p to unfolded protein stress are shown as a stick model with an atomic coloring scheme (carbon in white, nitrogen in blue, oxygen in red) and labeled. Dimer interface is indicated by gray dashed line. (B) Immunoblot of IRE1α and CNX (a loading control) from the parental S21 cells, the UPR-deficient IRE1α$^{\Delta LD15}$ clone, or IRE1α$^{\Delta LD15}$-derived clones rescued with a single allele of either the human wild-type (WT-3 and WT-16) or mutant IRE1α^{Y161A} luminal domain (Y161A-38 or Y161A-40; details as in Figure 3B). The migration of the parental hamster IRE1α (in the S21 cells, denoted IRE1) differs slightly from the human–hamster chimeric protein encoded by the rescued allele (IRE1^{hLD}). The protein encoded by the IRE1α$^{\Delta LD15}$ is considerably smaller (IRE1$^{\Delta LD}$). Blots are representative of at least two independent experiments. (C) Dose–response curve of UPR reporter expression in individual clones of IRE1α^{Y161A} mutant cells treated with Tm, 2DG, or PA at concentrations as in Figure 1A for 24 h. MFI for at least 9×10^3 cells was measured by flow cytometry. Curves were fitted to a four-parameter logistic model. Data are representative of at least two independent experiments (another experiment is shown in Supplemental Figure S6F). (D) Same as in C, except that data are shown as fold change relative to the reporter activity at lowest concentration of each stressor (set to a value of 1). Data are from one of two independent experiments performed (the second experiment is shown in Supplemental Figure S6G).

repair template encoding the IRE1α^{Y161A} mutation alongside the compound IRE1α$^{V437R;\ L441R}$, an IRE1α$^{\Delta 403\text{-}441}$ deletion (encompassing the predicted amphipathic helix), or IRE1α$^{TM>L}$, in which the TMD was replaced with a string of leucines (Figure 7, A and B). In the context of the IRE1α^{Y161A} modification, which biases IRE1α away from sensing unfolded proteins and allows the response to lipid aberrancy to dominate, all three mutants (IRE1α$^{V437R;\ L441R}$, IRE1α$^{\Delta 403\text{-}441}$, and IRE1α$^{TM>L}$) retained their ability to activate XBP1s::Turquoise reporter in palmitate-treated cells at levels similar to those of the reference IRE1α^{Y161A} mutant (Figure 7, C and D). Replacing the TMD residues of IRE1α with leucine (IRE1α$^{TM>L}$) sensitized IRE1α^{Y161A} to membrane aberrancy imposed by palmitate and to a lesser degree to tunicamycin (Figure 7, D and E). This feature of the compound *Ern1*$^{Y161A;\ TM>L}$ mutation, which was reproducibly observed in two independently isolated clones (Supplemental Figure S7), was all the more striking, given that the encoded compound mutant IRE1α$^{Y161A;TM>L}$ protein is expressed at lower levels than IRE1α^{Y161A}, which serves as a reference in this experiment (Figure 7A).

The experiments noted here point to an unanticipated robustness of IRE1α's ability to respond to lipid aberrancy by promoting the unconventional splicing of the XBP1s::Turquoise reporter. This was further examined by studying the response of endogenous XBP1 and its target genes in cells expressing the aforementioned IRE1α derivatives as their only source of IRE1α protein. The Y161A mutation selectively enfeebled the response to unfolded proteins also when assessed by IRE1α-mediated XBP1 splicing, although the defect was slightly less complete than that observed by the flow cytometry–based measurement of XBP1s::Turquoise activity (compare Figure 8A with Figure 6, C and D). In the context of the IRE1α^{Y161A} mutation, both IRE1α-dependent splicing of endogenous XBP1 mRNA (Figure 8, A and B, and Supplemental Figure S8) and the expression of two well-validated IRE1α-dependent UPR target

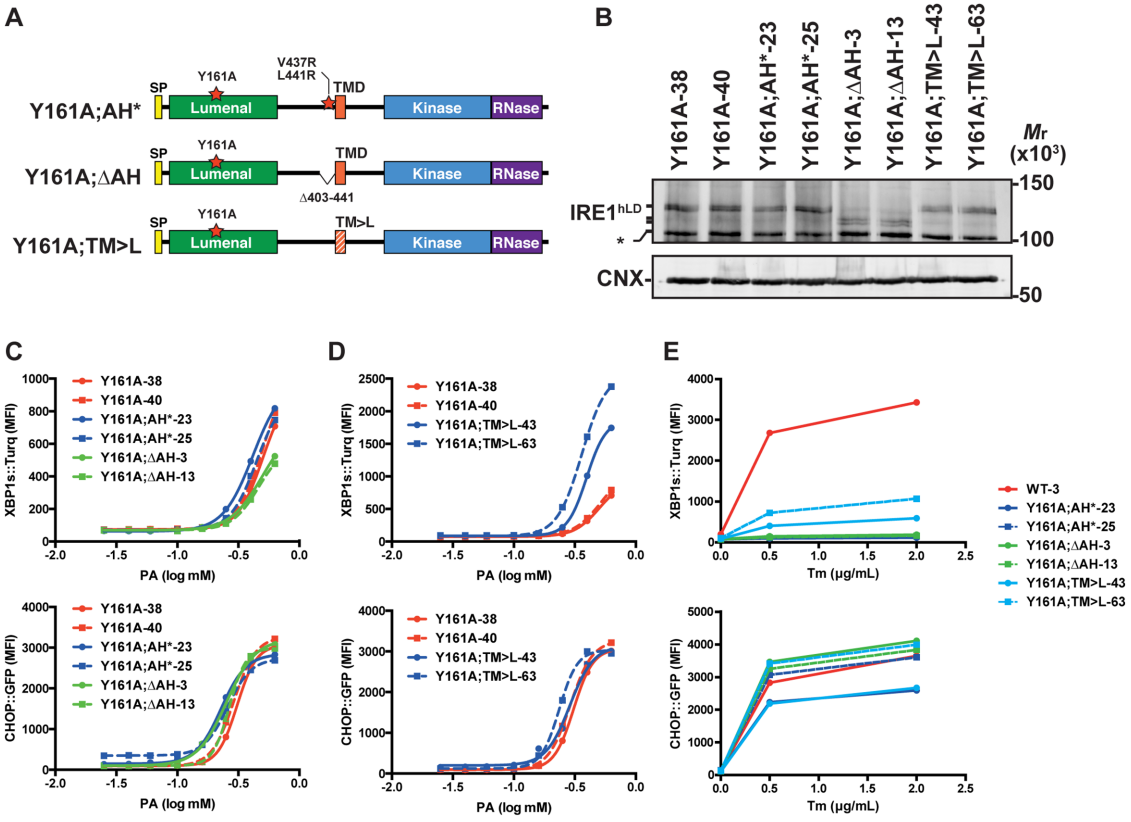

FIGURE 7: Robust induction of the UPR reporter by palmitate in cells expressing compound mutant IRE1α proteins that are unresponsive to unfolded protein stress. (A) Schema of Y161A-containing compound IRE1α mutants. IRE1α$^{Y161A;AH*}$ has additional IRE1α$^{V437R;\ L441R}$ mutations. IRE1α$^{Y161A;\Delta AH}$ has an additional deletion of 39 amino acid residues, IRE1α$^{\Delta 403\text{-}441}$, containing the predicted amphipathic helix (AH). The TMD of IRE1α $^{Y161A;TM>L}$ consists of only leucine residues (indicated by the striping of the orange box). Signal peptide (SP), yellow; core luminal domain, green; TMD, orange; kinase domain, cyan; RNase domain, purple. (B) Immunoblot of IRE1α and CNX (a loading control) from the mutant IRE1α^{Y161A} luminal domain clones (Y161A-38 or Y161A-40) and the compound mutants indicated (details as in Figure 3B). The migration of the human–hamster chimeric proteins is indicated (IRE1α^{hLD}), and an asterisk marks an irrelevant species. Note the slightly faster migration of the smaller IRE1α$^{Y161A;\Delta AH}$ protein. Blots are representative of at least two independent experiments. (C, D) Dose–response curve of UPR reporter expression in individual clones of IRE1α mutant cells treated with various concentrations of PA (0.025–0.63 mM) for 24 h. MFI for at least 9×10^3 cells was measured by flow cytometry. Curves were fitted to a four-parameter logistic model. Data are representative of at least two independent experiments (another experiment is shown in Supplemental Figure S7, A and B). (E) UPR reporter expression in individual clones of IRE1α mutant cells treated with various concentrations of Tm (0, 0.5, and 2 μg/ml) for 24 h. MFI for at least 9×10^3 cells was measured by flow cytometry. Data are representative of at least two independent experiments (another experiment is shown in Supplemental Figure S7C).

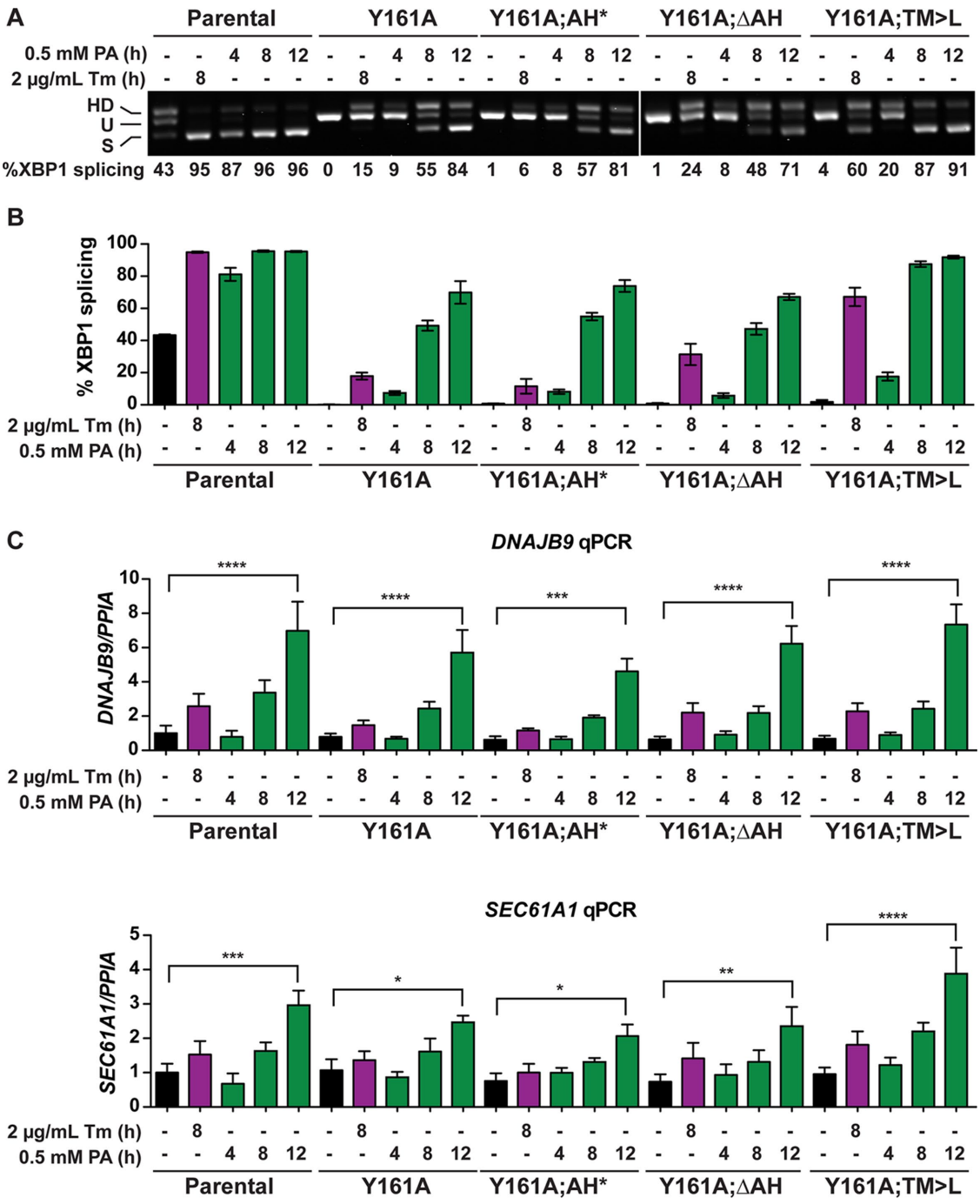

FIGURE 8: Robust induction of endogenous UPR markers by palmitate in cells expressing compound mutant IRE1α proteins that are unresponsive to unfolded protein stress. (A) Agarose gel of stained DNA fragments derived from XBP1 cDNA produced by reverse transcriptase PCR of mRNA from S21 (parental) and IRE1α mutant cells. The cells were untreated or treated with 0.5 mM PA or 2 μg/ml Tm as indicated. The unspliced (U) and spliced (S) products and heteroduplex species (HD) are indicated, and the fraction of spliced XBP1 mRNA in each sample is shown below the gel. Data are representative of three independent experiments (two other experiments are shown in Supplemental Figure S8). (B) Level of XBP1 splicing as determined by quantitation of the signals in A and Supplemental Figure S8. Data are mean ± SEM ($n = 3$). (C) Quantitative PCR analysis of mRNA expression levels of the XBP1 target genes *Dnajb9* and *Sec61a1* in S21 (parental) and IRE1α mutant cells treated as described. Values are normalized to *Ppia* (cyclophilin A) mRNA, a housekeeping gene, and represent mean ± SEM ($n = 3$). *$p < 0.05$; **$p < 0.01$; ***$p < 0.001$; ****$p < 0.0001$ (one-way analysis of variance, Bonferroni's post hoc test).

genes (*Dnajb9/ERdJ4* and *Sec61a1*; Shoulders *et al.*, 2013; Adamson *et al.*, 2016) were unaffected by secondary IRE1α$^{V437R;\ L441R}$, IRE1α$^{\Delta 403\text{-}441}$, or IRE1α$^{TM>L}$ mutations in palmitate-treated compound mutant cells (Figure 8C).

DISCUSSION

Changes in lipid membrane composition have long been known to affect UPR signaling. Similarly, a role for the TMD of the UPR transducers in recognizing the membrane aberrancy and in contributing to

changes in IRE1 and PERK activity in lipid-perturbed cells is well supported. Surprisingly, a previous study suggested that at least some of the molecular recognition events involved in IRE1α's response to membrane aberrancy proceeded despite rather drastic alterations to the sequence of the TMD (Volmer *et al.*, 2013). Here we extended the inquiry into features of IRE1α that endow it with the ability to recognize membrane aberrancy imposed by palmitate loading and rectified important limitations in previous studies. Our observations indicate that although the specialized conserved features of the IRE1α TMD do influence its responsiveness to membrane aberrancy, none is categorically required for UPR activation in palmitate-loaded cells.

The enzymatically active form of IRE1 is a dimer of its effector kinase endonuclease (KEN) domain, and a *trans*-autophosphorylation regulatory step followed by nucleotide binding precedes dimer formation of the cytosolic domain (Lee *et al.*, 2008). Both events are constrained by the plane of the ER membrane and, being bimolecular interactions, both are concentration dependent. Cooperativity between the steps associated with IRE1 activation and oligomerization of the protein in the plane of the membrane (Korennykh *et al.*, 2009) add up to nonlinear relationship between protein concentration and effector enzymatic activity (Korennykh *et al.*, 2011). For these reasons, analysis of IRE1 activity and the effects of mutants thereon must carefully consider the issue of protein concentration. The potentially corrupting effect of IRE1 overexpression is all the more acute, given the low abundance of IRE1 protein (Kim *et al.*, 2014). In yeast, the problem is compounded by lack of reagents to directly measure the presence of endogenous Ire1p and thereby assess the relative level of expression of derivatives.

Previous experiments in mammalian cells compared signaling in the IRE1-dependent branch of the UPR between overexpressed derivatives, and, even in yeast, where low–copy number plasmids were used, the degree of Ire1p expression remained indeterminate, as the endogenous protein remains undetectable (Promlek *et al.*, 2011; Volmer *et al.*, 2013). It was therefore impossible to conclude whether residual responsiveness to lipid perturbation observed in mutants that had lost the ability to respond to unfolded protein stress reflects a misleading experimental artifact or reports on features relevant to IRE1 signaling at endogenous levels of expression.

This study benefitted from recent developments in CRISPR/Cas9 technology that enable site-directed mutagenesis of the chromosomal copy of the gene of interest—in this case, the mammalian IRE1α encoding *Ern1* gene. None of the mutations in residues accounting for conserved features of IRE1α's TMD selectively desensitized the UPR transducer to palmitate loading. The activity of the IRE1α branch was assessed over the ascending portion of the concentration–response curve, avoiding the distorting effects of saturation. In most instances, the immunoblot signal arising from the mutant IRE1α proteins was found to be lower than that of the reference wild-type protein. These feeble signals likely reflected lower levels of expression in the cell. Altered immunogenicity of the mutant proteins was unlikely, as the immunogen used to raise the anti-IRE1α serum did not encompass the TMD (Bertolotti *et al.*, 2000). Altered extractability of the mutants into the detergent phase was rendered unlikely, as recovery was unaffected by including deoxycholate or low concentrations of SDS in the extracting buffer. Thus our findings speak against a role of the conserved features of IRE1α's TMD in sensitizing the transducer to membrane aberrancy.

The residual responsiveness to palmitate of IRE1α^{Y161A}, a luminal-domain mutant that lost much of its ability to respond to unfolded protein stress, occurs at physiological levels of expression. Regardless of whether this mutation attains its effect by lowering the affinity of IRE1α for activating unfolded protein ligands (Credle *et al.*, 2005) or by other means, its ability to neuter the response to unfolded protein stress provides an informative backdrop for the study of rationally designed second mutations to test their effect on IRE1α response to palmitate loading. The results point to a surprising robustness of IRE1α's ability to recognize membrane aberrancy. Even in the background of the IRE1α^{Y161A} mutation, none of the second mutations that we expected to desensitize IRE1α to lipid perturbation did so. Thus we can conclude firmly that although mammalian IRE1α possesses features that have been proven to promote favorable homotypic interactions between TMDs and thereby activation of Mga2p in ordered ER membranes (Covino *et al.*, 2016), these features are dispensable to the mammalian UPR.

Given the importance of dimerization to IRE1α activity, it seems reasonable to assume that recognition of membrane aberrancy has something to do with enhanced tendency of IRE1α's TMD to dimerize in lipid bilayers comprised of more saturated acyl chains. Simple biophysical principles may be at play. These include hydrophobic mismatch between TMD length and bilayer thickness, partitioning of IRE1α into lipid microdomains with differential effects on dimerization, and changes in strength of peptide–lipid interactions (reviewed in Volmer and Ron, 2015). The indifference of IRE1α to alterations in the composition of its TMD does not help discriminate among the various possibilities. Similarly limited is the inference one can draw from comparing the wild-type IRE1α to the IRE1α^{Y161A}, a mutant defective in its ability to respond to unfolded protein stress. If the mutant were purely defective in recognizing an unfolded protein stress signal (but intact in all other respects), one could infer that most of the increase in IRE1α signaling in palmitate-loaded cells arises from the secondary induction of unfolded protein stress, as the IRE1α^{Y161A} mutant remains markedly impaired in its response to palmitate. However, the mutant is also expressed at lower levels than the wild type and may well manifest features that impair the response to membrane aberrancy independently of the mutation's effect on recognizing the unfolded protein stress signal; for example, Y161A might lower the intrinsic affinity of IRE1α luminal domain protomers for one another.

Our findings do suggest that stripping IRE1α TMD of its conserved features correlated with lower levels of expression and a pattern of enhanced sensitivity to palmitate loading. However, the conclusion that conserved features found in IRE1α's TMD (and TMD-proximal segment) might have evolved to tune the protein to lower activity in lipid perturbed cells should be made tentatively. First, the statistical sample of IRE1α mutants tested in this study remains small—even with the power of CRISPR/Cas9, elaborating and characterizing informative chromosomal mutations is laborious. Second, the most pronounced gain-of-function features (over the wild type) were observed in the case of the IRE1α$^{TM>L}$. Although this mutant certainly strips IRE1α TMD of all its special features, it may also have acquired special gain-of-function features, such as the tendency to form a leucine zipper (Brooks *et al.*, 2014) and thereby favor IRE1 dimerization. Third, our analysis has been confined to one kind of lipid perturbation, namely, loading cells with the saturated fatty acid palmitate. It is possible that the features of IRE1α altered here play a role in detecting membrane aberrancy caused by alteration in other membrane constituents. Furthermore, our conclusions are limited to mammalian IRE1α; the IRE1β isoform of mammals and the single IRE1 protein of other animal species, yeasts, and protists may obey different rules. Perhaps the greatest value of this study is therefore in highlighting shortcomings in our ability to bioinformatically predict conserved mechanisms that sense membrane aberrancy and to showcase an effective experimental method for exploring this process as it relates to one branch of the UPR.

MATERIALS AND METHODS

Plasmid construction

A combination of PCR-based manipulations, restriction digests, and site-directed mutagenesis procedures was used to create DNA constructs. Supplemental Table S1 lists the plasmids used, their lab names, description, and published reference where available.

Preparation of palmitate–bovine serum albumin complex

Palmitate–bovine serum albumin (BSA) complex was prepared by modification of a published method (Spector, 1986). Briefly, a 20 mM solution of sodium palmitate (P9767; Sigma-Aldrich, United Kingdom) in 0.01 M NaOH was incubated at 70°C for 30 min. Prewarmed palmitate solution was added dropwise to 20% fatty acid–free BSA (A6003; Sigma-Aldrich) in phosphate-buffered saline (PBS) at a 6.6:1 palmitate-to-BSA molar ratio. The resultant palmitate–BSA complex solution was filtered, aliquoted, and stored at −20°C.

Cell culture and treatment

CHO-K1–based cell lines were maintained in regular medium consisting of Nutrient Mixture F-12 Ham (Sigma-Aldrich), 10% fetal calf serum (FCS; FetalClone II, Lot ABB214492; Hyclone-GE Healthcare Life Sciences, South Logan, UT), 2 mM L-glutamine (Sigma-Aldrich), and 1× penicillin/streptomycin (Sigma-Aldrich) at 37°C with 5% CO_2. HEK293T cells were cultured in DMEM (Sigma-Aldrich) supplemented as described.

Cells were treated with drugs at the following final concentrations: 0.080–2.0 µg/ml tunicamycin (Melford, United Kingdom), 0.13–16 mM 2DG; Acros Organics, Belgium), 0.025–0.63 mM palmitate (as a BSA complex; see earlier description), and 6-8 µg/ml puromycin (Calbiochem, La Jolla, CA). All drugs were first diluted in fresh, prewarmed medium and then applied to the cells by medium exchange. For palmitate treatment, 1% FCS medium was used.

Generation of the genome edited cells by CRISPR/Cas9

ΔTM12 cells. Two single-guide RNA (sgRNA) sequences for targeting exon 12 of *Cricetulus griseus* (Chinese hamster) *Ern1* were selected from the CRISPy database (http://staff.biosustain.dtu.dk/laeb/crispy/; Ronda *et al.*, 2014), and duplex DNA oligonucleotides (made of oligo DNAs 1155/1156 and 1157/1158 in Supplemental Table S2) of the sequences were inserted into the pSpCas9(BB)-2A-Puro plasmid (plasmid UK1367) to create sgRNA/Cas9 plasmids UK1588 and UK1589, respectively by following published procedures (Ran *et al.*, 2013; Cong and Zhang, 2015).

CHO-K1 XBP1s::Turquoise/CHOP::GFP dual reporter cells (S21 cells; Sekine *et al.*, 2016) were plated in six-well plates (Corning, Corning, NY) at a density of 2×10^5 per well. Twenty-four hours later, the cells were transfected with sgRNA/Cas9 plasmids UK1588 and UK1589 (1 µg each per transfection) using Lipofectamine LTX (Invitrogen, United Kingdom). Forty-eight hours after transfection, the cells were plated in 10-cm dishes (Corning) at 2.5×10^6 cells. Twenty-four hours later, cells were treated with 4 mM 2DG and further incubated for 24 h. The 2DG-treated cells were washed with PBS and resuspended in PBS containing 4 mM EDTA and 0.5% (wt/vol) BSA, and an XBP1s::Turquoise^{dim}, CHOP::GFP^{high} population was individually sorted by FACS into 96-well plates (Corning) using a MoFlo Cell Sorter (Beckman Coulter, Fullerton, CA).

Clones were then analyzed by a PCR-based assay to detect *Ern1* mutations, as described (Klampfl *et al.*, 2013). Briefly, primers (1193 and 1189) were designed for the region encompassing the *Ern1* sgRNA target sites, and the forward primer was labeled with 6-carboxyfluorescein (6-FAM) on the 5′ end. A PCR was set up using 0.1 µl of Phusion High-Fidelity DNA Polymerase (New England Biolabs, Ipswich, MA), 0.5 µl of 10 µM labeled forward and reverse primers, 2 µl of 5× buffer, 0.2 µl of 2.5 mM dNTPs, 5.7 µl of H_2O, and 1 µl of proteinase K–digested cell lysate (used as a crude genomic DNA). PCR was performed as follows: 98°C for 30 s, 30× (98°C for 10 s, 65°C for 20 s, 72°C for 30 s), and 72°C for 10 min. PCR products were diluted 1:50 or 1:200 in water, fragment length was determined on a 3130xl Genetic Analyzer (Applied Biosystems, United Kingdom), and the data were analyzed using the Gene Mapper software (Applied Biosystems).

Clones for which frameshift-causing insertions or deletions (InDels) were detected for both alleles (based on PCR fragment size) were sequenced to confirm the *Ern1* mutations.

Knock-in of TMD by CRISPR/Cas9-mediated homology-directed repair. A series of mutations in IRE1 TM domain was reconstituted in ΔTM12 cells by a CRISPR/Cas9-mediated homology-directed repair (HDR).

An sgRNA sequence for targeting the exon 12 of *Ern1* was selected from the CRISPy database, and a duplex DNA oligonucleotide (made of oligo DNAs 1193 and 1189) of the sequence was inserted into the pSpCas9(BB)-2A-mCherry plasmid (plasmid UK1610) to create the sgRNA/Cas9 plasmid UK1615.

To construct a wild-type repair template (UK1837) that contains TMD-coding exon 12, a 2969–base pair CHO genomic fragment containing exon 12 of *Ern1* was amplified by PCR using primers 1136 and 1139, digested with *Kpn*I and *Sac*I, and ligated into *Kpn*I/*Sac*I-digested pBluescript II KS(+) plasmid (pBS KS(+); UK1). The sequence targeted by sgRNA of UK1615 in the repair template was mutated by site-directed mutagenesis using primers 1604 and 1605.

Repair templates for TM>L (UK1910), TM-FWY>L (UK1911), W464L (UK1912), P472A (UK1913), and G463L/A466L (UK1914) were created by site-directed mutagenesis of UK1837 using primers 1695 and 1696 for UK1910, 1697 and 1698 for UK1911, 1701 and 1702 for UK1912, 1699 and 1700 for UK1913, and 1705 and 1706 for UK1914.

To construct a repair template for scrambling TMD (UK1838), 5′ and 3′ homology arms amplified by primers 1136/1137 and 1138/1139, respectively, were PCR knitted by primers 1136 and 1139. The resultant DNA fragment was digested with *Kpn*I and *Sac*I and ligated into *Kpn*I/*Sac*I-digested pBS KS(+).The sequence targeted by sgRNA of UK1615 in the repair template was mutated by site-directed mutagenesis using primers 1606 and 1607.

ΔTM12 cells were plated in six-well plates at a density of 2×10^5 per well. Twenty-four hours later, the cells were transfected with sgRNA/Cas9 plasmid UK1615 together with a repair template (1 µg each per transfection) using Lipofectamine LTX. Forty-eight hours after transfection, the cells were plated in 10-cm dishes at 2.5×10^6 cells. Twenty-four hours later, cells were treated with 4 mM 2DG and further incubated for 24 h. The 2DG-treated cells were washed with PBS and resuspended in PBS containing 4 mM EDTA and 0.5% (wt/vol) BSA, and an XBP1s::Turquoise^{high}, CHOP::GFP^{high} population was sorted into six-well plates as a polyclonal pool and also sorted individually into 96-well plates by FACS using a MoFlo Cell Sorter.

The size of DNA fragments amplified from genomic DNA of each clone by PCR using primers 1193 and 1189 was analyzed using a 3130xl Genetic Analyzer and Gene Mapper software as described earlier. Clones that showed the same DNA fragment size as wild-type *Ern1* were regarded as cells in which both alleles were correctly edited and then sequenced to confirm the editing (Supplemental Figure S9).

ΔLD15 cells. An sgRNA sequence for targeting the exon 2 of *C. griseus Ern1* was selected from the CRISPy database, and a duplex DNA oligonucleotide (made of oligo DNAs 1608 and 1609) of the sequence was inserted into the pSpCas9(BB)-2A-Puro plasmid (plasmid UK1367) to create sgRNA/Cas9 plasmid UK1848.

S21 cells were plated in six-well plates at a density of 2×10^5 per well. Twenty-four hours later, the cells were transfected with sgRNA/Cas9 plasmids UK1615 and UK1848 (1 μg each per transfection) using Lipofectamine LTX. Forty-eight hours after transfection, the cells were plated in 10-cm dishes at 2.5×10^6 cells. Twenty-four hours later, cells were treated with 4 mM 2DG and further incubated for 24 h. The 2DG-treated cells were washed with PBS, resuspended in PBS containing 4 mM EDTA, and 0.5% (wt/vol) BSA, and an XBP1s::Turquoise^{dim}, CHOP::GFP^{high} population was individually sorted by FACS into 96-well plates using a MoFlo Cell Sorter.

Clones that have an ~50-kb deletion were screened by PCR using a primer set (1643 and 1189) flanking exons 2–12 of *Ern1* (see Supplemental Figure S6A). A PCR was set up using 0.3 μl of Taq DNA Polymerase (New England Biolabs), 0.5 μl of 10 μM forward and reverse primers, 2 μl of 10× buffer, 1.6 μl of 2.5 mM dNTPs, 14.5 μl of H_2O, and 1 μl of crude genomic DNA. Clones for which an ~50-kb deletion was detected were further evaluated for the presence of an allele that does not have an ~50-kb deletion between exons 2 and 12 by PCR using a primer pair flanking exon 2 (1643 and 1644) or exon 12 (1188 and 1189).

Clones that apparently have an ~50-kb deletion in both alleles were selected and sequenced to confirm the *Ern1* mutations. One allele of ΔLD15 clone has an in-frame fusion exon of exons 2 and 12, and the other allele has a larger deletion predicted to be null.

"Knock-in" of human IRE1α luminal domain–encoding cDNA-based "minigene" by CRISPR/Cas9-mediated HDR. A series of mutations in the IRE1α luminal domain (LD) and/or amphipathic helix was reconstituted in ΔLD15 cells by a CRISPR/Cas9-mediated HDR.

An sgRNA sequence for targeting the fusion of exons 2 and 12 of *Ern1* in ΔLD15 cells was designed, and a duplex DNA oligonucleotide (1691 and 1692) of the sequence was inserted into the pSpCas9(BB)-2A-mCherry plasmid (plasmid UK1610) to create sgRNA/Cas9 plasmid UK1903.

To construct a repair template containing a cDNA of human IRE1α LD, 5′ and 3′ homology arms were amplified from CHO genomic DNA by PCR using the primers 1713/1683 and 1684/1139, respectively. A cDNA of human IRE1α LD (amino acids 30–446) was amplified from the hIRE1a_V1_pBS plasmid (UK154) by PCR using primers 1681 and 1682. Homology arms and a DNA fragment containing human IRE1α LD cDNA were PCR knitted by primers 1713 and 1139. The resultant 3447-–base pair DNA fragment was cloned into pCR-BluntII-TOPO vector (Invitrogen) to create the CHO_IRE1_hIRE1-LD_reptemp4_pCR-Blunt2-TOPO (UK1968) wild-type repair template.

Repair templates for Y161A (UK1971), V437R (UK2016), and L441R (UK2017) were created by site-directed mutagenesis of UK1968 using primers1736 and 1737 for UK1971, 1833 and 1834 for UK2016, and 1835 and 1836 for UK2017.

Repair templates for Y161A;V437R;L441R (UK2029) and Y161A;TM>L (UK2031) were created by site-directed mutagenesis of UK1971 using primers1852 and 1853 for UK2029 and 1695 and 1696 for UK2031.

To create a repair template for Y161A;Δ403-441 (UK2030), UK1968 was linearized by PCR using primers 1830 and 1829, and then a 343–base pair synthetic DNA fragment (gBlock; IDT, Coralville, IA) was cloned into linearized UK1968 by the Gibson assembly method (Gibson *et al.*, 2009) to create CHO_IRE1_hIRE1-LD_rVdel_pCR (UK2018). The Y161A mutation was introduced into UK2018 by site-directed mutagenesis of UK2018 using primers 1736 and 1737 for UK2029. The gBlock sequence used was 5′-TGCTGGAAGGGCCCCAGACTGATGGCGTCACCATC-GGGGACAAGGGGGAGTGTGTGATCACGCCCAGCACGGAC-GTCAAGTTTGATCCCGGACTCAAAAGCAAGAACAAGCTCAAC-TACTTGAGGAATTACTGGCTTCTGATAGGACACCAT-GAAACCCCACTGTCTGCGTCTACCAAGATGCTGGAGAGA-TTTCCCAACAATCTACCCAAACATCGGGAAAATGTGATTCCT-GCTGATTCAGAGAAAAAGAGCTTTGAGGAAAAGGACATGGC-TACTATTATCCTGAGCACCTTCCTGCTGGTTGGATGGGTG-GCCTTCATCATCACTTACCCCCTGGTAA-3′.

ΔLD15 cells were plated in six-well plates at a density of 2×10^5 per well. Twenty-four hours later, the cells were transfected with an sgRNA/Cas9 plasmid UK1903 (0.12 μg per transfection) together with a repair template (1.9 μg per transfection) using Lipofectamine LTX. Forty-eight hours after transfection, the cells were plated in 10-cm dishes at 2.5×10^6 cells. Twenty-four hours later, cells were treated with 4 mM 2DG and further incubated for 24 h. The 2DG-treated cells were washed with PBS and resuspended in PBS containing 4 mM EDTA and 0.5% (wt/vol) BSA, and an XBP1s::Turquoise^{high}, CHOP::GFP^{high} population was sorted individually into 96-well plates by FACS using a MoFlo Cell Sorter. In the case of IRE1α mutations that impair 2DG-induced XBP1s::Turquoise expression, cells expressing mCherry (transfection marker of sgRNA/Cas9 plasmid) were sorted individually into 96-well plates. Clones were analyzed by PCR using primers 1643 and 1189 to detect human IRE1α LD cDNA reconstituted in the *Ern1* genomic locus. Correctly edited clones were sequenced to confirm the editing (Supplemental Figure S9).

Flow cytometry analysis

S21 cells and their derivatives were plated at a density of 1×10^5 cells per well on 12-well plates. On the next day, the culture medium was replaced with 1 ml of fresh medium, and cells were treated with indicated compounds for 24 h. Immediately before analysis, the cells were washed with PBS and collected in PBS containing 4 mM EDTA. Single-cell fluorescence signals (10,000 cells/sample) were measured by a dual-channel flow cytometry with an LSRFortessa cell analyzer (Becton Dickinson, Franklin Lakes, NJ). GFP (excitation laser 488 nm, filter 530/30) and Turquoise (modified cyan fluorescent protein; excitation laser 405 nm, filter 450/50) signals were detected. FlowJo software (FlowJo, Ashland, OR) was used to analyze the data.

Immunoprecipitation and immunoblot

Membrane-associated proteins were prepared from digitonin-permeabilized cells as previously described (Le Gall *et al.*, 2004), with some modifications. Three 10-cm dishes of confluent cells were washed with PBS, harvested with PBS containing 4 mM EDTA, centrifuged at $400 \times g$ for 5 min at 4°C, and washed with HCN buffer (50 mM 4-(2-hydroxyethyl)-1-piperazineethanesulfonic acid [HEPES], pH 7.5, 150 mM NaCl, 2 mM $CaCl_2$). Cells were then resuspended in 1.5 ml of HCN buffer containing 0.09% (wt/vol) digitonin (300410; Calbiochem) and incubated on ice for 10 min. The digitonin-permeabilized cells were centrifuged ($1000 \times g$ for 5 min at 4°C), washed twice with HNE buffer (50 mM HEPES, pH 7.5, 150 mM NaCl, 1 mM ethylene glycol tetraacetic acid), lysed in a lysis buffer (1% Triton X-100, 50 mM Tris-HCl, pH 7.4, 150 mM NaCl, 1 mM EDTA, 10% glycerol, 2 mM phenylmethylsulfonyl fluoride, 10 μg/ml aprotinin, 4 μg/μl pepstatin, 4 μM leupeptin, 10 mM sodium pyrophosphate, 100 mM NaF, 17.5 mM β-glycerophosphate) on ice for 5 min. The lysates were cleared for 10 min at $21,000 \times g$ at 4°C. Bio-Rad protein

assay reagent (BioRad, Richmond, CA) was used to determine the protein concentrations of lysates, followed by normalization. Supplemental Figure S10 presents an experimental analysis of the extractability of wild-type and mutant IRE1α.

For immunoprecipitation of IRE1α protein, 20 µl of protein A–Sepharose (Invitrogen) and 1 µl of anti-IRE1α rabbit polyclonal antibody (NY200; Bertolotti *et al.*, 2000) were added to cell lysates and rotated overnight at 4°C. The beads were washed in 0.6 ml of lysis buffer three times. The beads were mixed with 40 µl of 2 × SDS-sample buffer and incubated at 70°C for 10 min. After spinning down of beads, supernatant was collected and subjected to immunoblot analysis.

A 20-µl amount of immunoprecipitated samples or 20–40 µg of protein of lysates was subjected to 7% SDS–PAGE and transferred onto Immobilon-P polyvinylidene fluoride membrane (Merck Millipore, Bedford, MA). Membranes were blocked with 5% (wt/vol) dried skimmed milk in TBS (25 mM Tris-HCl, pH 7.5, 150 mM NaCl) and incubated with primary antibodies, followed by IRDye fluorescently labeled secondary antibodies (LiCor, Lincoln, NE). The membranes were scanned with an Odyssey near-infrared imager (LiCor). Primary antibodies and antisera against IRE1α (NY200; Bertolotti *et al.*, 2000), calnexin (ab22595; Abcam, Cambridge, United Kingdom), and hamster BiP (Avezov *et al.*, 2013) were used.

XBP1 splicing assay and quantitative real-time PCR

Total RNA was isolated from cells by acid guanidinium thiocyanate-phenol-chloroform extraction using RNA STAT 60 (Amsbio, Lake Forest, CA) and isopropanol precipitation. A 2-µg amount of RNA was reverse transcribed by a reverse transcriptase RevertAid (ThermoFisher Scientific, Grand Island, NY) with oligo(dT)18 primer.

For XBP1 splicing assay, unspliced and spliced *Xbp1* cDNA fragments were amplified by PCR using primers 5 and 1470 and separated by 4% agarose gel containing SYTO60 (Invitrogen). Gels were visualized and quantified using an Odyssey near-infrared imager. The percentage of XBP1 splicing was calculated using the equation

$$\text{XBP1 splicing } (\%) = \frac{I(\text{XBP1s}) + \frac{1}{2} I\left(\text{XBP1}^{\text{HD}}\right)}{I(\text{XBP1u}) + I(\text{XBP1s}) + I\left(\text{XBP1}^{\text{HD}}\right)} \times 100$$

where *I*(XBP1u), *I* (XBP1s), and *I* (XBP1^{HD}) indicate band intensities of unspliced XBP1, spliced XBP1, and a heteroduplex of unspliced and spliced XBP1, respectively.

Quantitative PCR analysis was performed using Power SYBR Green PCR Master Mix (Applied Biosystems) according to the manufacturer's instruction on a 7900HT Fast Real-Time PCR system (Applied Biosystems). Oligo DNAs in Supplemental Table S2 were used for PCR: 1929 and 1930 for *Dnajb9*, 1931 and 1932 for *Sec61a1*, and 1487 and 1488 for *Ppia*. Relative quantities of amplified PCR products were determined using SDS 2.4.1 software (Applied Biosystems) and normalized to *Ppia* values.

ACKNOWLEDGMENTS

We thank H. Sharpe (Cambridge Institute for Medical Research) for advice on construction of membrane-spanning mutants and insightful comments on the manuscript; R. Ernst and K. Halbleib (Goethe-University, Frankfurt, Germany) for discussing unpublished experimental observations and providing constructive critiques on the manuscript; R. Schulte and the Cambridge Institute for Medical Research flow cytometry team for assistance; and S. Preissler, C. Rato, and R. Saunders (Cambridge Institute for Medical Research) for advice and comments on the manuscript. This work was supported by grants from the Wellcome Trust (Wellcome 200848/Z/16/Z and strategic award Wellcome 100140) and a Medical Research Council studentship to N.A.-W. (MR/K50127X/1). D.R. is a Wellcome Trust Principal Research Fellow.

REFERENCES

Adamson B, Norman TM, Jost M, Cho MY, Nunez JK, Chen Y, Villalta JE, Gilbert LA, Horlbeck MA, Hein MY, *et al.* (2016). A multiplexed single-cell CRISPR screening platform enables systematic dissection of the unfolded protein response. Cell 167, 1867–1882e21.

Ariyama H, Kono N, Matsuda S, Inoue T, Arai H (2010). Decrease in membrane phospholipid unsaturation induces unfolded protein response. J Biol Chem 285, 22027–22035.

Avezov E, Cross BC, Kaminski Schierle GS, Winters M, Harding HP, Melo EP, Kaminski CF, Ron D (2013). Lifetime imaging of a fluorescent protein sensor reveals surprising stability of ER thiol redox. J Cell Biol 201, 337–349.

Bertolotti A, Zhang Y, Hendershot L, Harding H, Ron D (2000). Dynamic interaction of BiP and the ER stress transducers in the unfolded protein response. Nat Cell Biol 2, 326–332.

Brooks AJ, Dai W, O'Mara ML, Abankwa D, Chhabra Y, Pelekanos RA, Gardon O, Tunny KA, Blucher KM, Morton CJ, *et al.* (2014). Mechanism of activation of protein kinase JAK2 by the growth hormone receptor. Science 344, 1249783.

Cong L, Zhang F (2015). Genome engineering using CRISPR-Cas9 system. Methods Mol Biol 1239, 197–217.

Contreras FX, Ernst AM, Haberkant P, Bjorkholm P, Lindahl E, Gonen B, Tischer C, Elofsson A, von Heijne G, Thiele C, *et al.* (2012). Molecular recognition of a single sphingolipid species by a protein's transmembrane domain. Nature 481, 525–529.

Coskun U, Grzybek M, Drechsel D, Simons K (2011). Regulation of human EGF receptor by lipids. Proc Natl Acad Sci USA 108, 9044–9048.

Covino R, Ballweg S, Stordeur C, Michaelis JB, Puth K, Wernig F, Bahrami A, Ernst AM, Hummer G, Ernst R (2016). A eukaryotic sensor for membrane lipid saturation. Mol Cell 63, 49–59.

Cox JS, Chapman RE, Walter P (1997). The unfolded protein response coordinates the production of endoplasmic reticulum protein and endoplasmic reticulum membrane. Mol Biol Cell 8, 1805–1814.

Credle JJ, Finer-Moore JS, Papa FR, Stroud RM, Walter P (2005). On the mechanism of sensing unfolded protein in the endoplasmic reticulum. Proc Natl Acad Sci USA 102, 18773–18784.

Cunha DA, Hekerman P, Ladriere L, Bazarra-Castro A, Ortis F, Wakeham MC, Moore F, Rasschaert J, Cardozo AK, Bellomo E, *et al.* (2008). Initiation and execution of lipotoxic ER stress in pancreatic beta-cells. J Cell Sci 121, 2308–2318.

Cybulski LE, Martin M, Mansilla MC, Fernandez A, de Mendoza D (2010). Membrane thickness cue for cold sensing in a bacterium. Curr Biol 20, 1539–1544.

Deguil J, Pineau L, Rowland Snyder EC, Dupont S, Beney L, Gil A, Frapper G, Ferreira T (2011). Modulation of lipid-induced ER stress by fatty acid shape. Traffic 12, 349–362.

Feng B, Yao PM, Li Y, Devlin CM, Zhang D, Harding HP, Sweeney M, Rong JX, Kuriakose G, Fisher EA, *et al.* (2003). The endoplasmic reticulum is the site of cholesterol-induced cytotoxicity in macrophages. Nat Cell Biol 5, 781–792.

Fu S, Yang L, Li P, Hofmann O, Dicker L, Hide W, Lin X, Watkins SM, Ivanov AR, Hotamisligil GS (2011). Aberrant lipid metabolism disrupts calcium homeostasis causing liver endoplasmic reticulum stress in obesity. Nature 473, 528–531.

Gibson DG, Young L, Chuang RY, Venter JC, Hutchison CA 3rd, Smith HO (2009). Enzymatic assembly of DNA molecules up to several hundred kilobases. Nat Methods 6, 343–345.

Gil G, Faust JR, Chin DJ, Goldstein JL, Brown MS (1985). Membrane-bound domain of HMG CoA reductase is required for sterol-enhanced degradation of the enzyme. Cell 41, 249–258.

Halbleib K, Pesek K, Covino R, Hofbauer HF, Wunnicke D, Hänelt I, Hummer G, Ernst R (2017). Activation of the unfolded protein response by lipid bilayer stress. Mol Cell 67, 1–12.

Han J, Kaufman RJ (2016). The role of ER stress in lipid metabolism and lipotoxicity. J Lipid Res 57, 1329–1338.

Iwawaki T, Akai R, Kohno K, Miura M (2004). A transgenic mouse model for monitoring endoplasmic reticulum stress. Nat Med 10, 98–102.

Jonikas MC, Collins SR, Denic V, Oh E, Quan EM, Schmid V, Weibezahn J, Schwappach B, Walter P, Weissman JS, Schuldiner M (2009).

Comprehensive characterization of genes required for protein folding in the endoplasmic reticulum. Science 323, 1693–1697.
Kim MS, Pinto SM, Getnet D, Nirujogi RS, Manda SS, Chaerkady R, Madugundu AK, Kelkar DS, Isserlin R, Jain S, *et al.* (2014). A draft map of the human proteome. Nature 509, 575–581.
Klampfl T, Gisslinger H, Harutyunyan AS, Nivarthi H, Rumi E, Milosevic JD, Them NC, Berg T, Gisslinger B, Pietra D, *et al.* (2013). Somatic mutations of calreticulin in myeloproliferative neoplasms. N Engl J Med 369, 2379–2390.
Korennykh AV, Egea PF, Korostelev AA, Finer-Moore J, Stroud RM, Zhang C, Shokat KM, Walter P (2011). Cofactor-mediated conformational control in the bifunctional kinase/RNase Ire1. BMC Biol 9, 48.
Korennykh AV, Egea PF, Korostelev AA, Finer-Moore J, Zhang C, Shokat KM, Stroud RM, Walter P (2009). The unfolded protein response signals through high-order assembly of Ire1. Nature 457, 687–693.
Lee AG (2011). Lipid-protein interactions. Biochem Soc Trans 39, 761–766.
Le Gall S, Neuhof A, Rapoport T (2004). The endoplasmic reticulum membrane is permeable to small molecules. Mol Biol Cell 15, 447–455.
Lee KPK, Dey M, Neculai D, Cao C, Dever TE, Sicheri F (2008). Structure of the dual enzyme Ire1 reveals the basis for catalysis and regulation in non-conventional RNA splicing. Cell 132, 89–100.
Li Y, Ge M, Ciani L, Kuriakose G, Westover EJ, Dura M, Covey DF, Freed JH, Maxfield FR, Lytton J, Tabas I (2004). Enrichment of endoplasmic reticulum with cholesterol inhibits sarcoplasmic-endoplasmic reticulum calcium ATPase-2b activity in parallel with increased order of membrane lipids: implications for depletion of endoplasmic reticulum calcium stores and apoptosis in cholesterol-loaded macrophages. J Biol Chem 279, 37030–37039.
Nikawa J, Yamashita S (1992). IRE1 encodes a putative protein kinase containing a membrane-spanning domain and is required for inositol phototrophy in Saccharomyces cerevisiae. Mol Microbiol 6, 1441–1446.
Novoa I, Zeng H, Harding H, Ron D (2001). Feedback inhibition of the unfolded protein response by GADD34-mediated dephosphorylation of eIF2a. J Cell Biol 153, 1011–1022.
Pineau L, Colas J, Dupont S, Beney L, Fleurat-Lessard P, Berjeaud JM, Berges T, Ferreira T (2009). Lipid-induced ER stress: synergistic effects of sterols and saturated fatty acids. Traffic 10, 673–690.
Promlek T, Ishiwata-Kimata Y, Shido M, Sakuramoto M, Kohno K, Kimata Y (2011). Membrane aberrancy and unfolded proteins activate the endoplasmic reticulum stress sensor Ire1 in different ways. Mol Biol Cell 22, 3520–3532.
Ran FA, Hsu PD, Wright J, Agarwala V, Scott DA, Zhang F (2013). Genome engineering using the CRISPR-Cas9 system. Nat Protoc 8, 2281–2308.
Robblee MM, Kim CC, Porter Abate J, Valdearcos M, Sandlund KL, Shenoy MK, Volmer R, Iwawaki T, Koliwad SK (2016). Saturated fatty acids engage an IRE1alpha-dependent pathway to activate the NLRP3 inflammasome in myeloid cells. Cell Rep 14, 2611–2623.
Ronda C, Pedersen LE, Hansen HG, Kallehauge TB, Betenbaugh MJ, Nielsen AT, Kildegaard HF (2014). Accelerating genome editing in CHO cells using CRISPR Cas9 and CRISPy, a web-based target finding tool. Biotechnol Bioeng 111, 1604–1616.
Russ WP, Engelman DM (2000). The GxxxG motif: a framework for transmembrane helix-helix association. J Mol Biol 296, 911–919.
Sekine Y, Zyryanova A, Crespillo-Casado A, Amin-Wetzel N, Harding HP, Ron D (2016). Paradoxical sensitivity to an integrated stress response blocking mutation in vanishing white matter cells. PLoS One 11, e0166278.
Sharpe HJ, Stevens TJ, Munro S (2010). A comprehensive comparison of transmembrane domains reveals organelle-specific properties. Cell 142, 158–169.
Shoulders MD, Ryno LM, Genereux JC, Moresco JJ, Tu PG, Wu C, Yates JR 3rd, Su AI, Kelly JW, Wiseman RL (2013). Stress-independent activation of XBP1s and/or ATF6 reveals three functionally diverse ER proteostasis environments. Cell Rep 3, 1279–1292.
Spector AA (1986). Structure and lipid binding properties of serum albumin. Methods Enzymol 128, 320–339.
Sriburi R, Jackowski S, Mori K, Brewer JW (2004). XBP1: a link between the unfolded protein response, lipid biosynthesis and biogenesis of the endoplasmic reticulum. J Cell Biol 167, 35–41.
Sundaram A, Plumb R, Appathurai S, Mariappan M (2017). The Sec61 translocon limits IRE1alpha signaling during the unfolded protein response. Elife 6, e27187.
Surma MA, Klose C, Peng D, Shales M, Mrejen C, Stefanko A, Braberg H, Gordon DE, Vorkel D, Ejsing CS,, *et al.* (2013). A lipid E-MAP identifies Ubx2 as a critical regulator of lipid saturation and lipid bilayer stress. Mol Cell 51, 519–530.
Thibault G, Shui G, Kim W, McAlister GC, Ismail N, Gygi SP, Wenk MR, Ng DT (2012). The membrane stress response buffers lethal effects of lipid disequilibrium by reprogramming the protein homeostasis network. Mol Cell 48, 16–27.
Travers KJ, Patil CK, Wodicka L, Lockhart DJ, Weissman JS, Walter P (2000). Functional and genomic analyses reveal an essential coordination between the unfolded protein response and ER-associated degradation. Cell 101, 249–258.
Volmer R, Ron D (2015). Lipid-dependent regulation of the unfolded protein response. Curr Opin Cell Biol 33, 67–73.
Volmer R, van der Ploeg K, Ron D (2013). Membrane lipid saturation activates endoplasmic reticulum unfolded protein response transducers through their transmembrane domains. Proc Natl Acad Sci USA 110, 4628–4633.
Zhou J, Liu CY, Back SH, Clark RL, Peisach D, Xu Z, Kaufman RJ (2006). The crystal structure of human IRE1 luminal domain reveals a conserved dimerization interface required for activation of the unfolded protein response. Proc Natl Acad Sci USA 103, 14343–14348.